ELSEVIER

Computers & Geosciences 32 (2006) 1758–1768

COMPUTERS & GEOSCIENCES

www.elsevier.com/locate/cageo

Addition of simultaneous heat and solute transport and variable fluid viscosity to SEAWAT ☆

Danny Thorne[a], Christian D. Langevin[b], Michael C. Sukop[c,*]

[a]Department of Mathematics, Physics and Computer Science, Georgetown College, 400 E. College Street, Georgetown, KY 40324, USA
[b]United States Geological Survey, 3110 SW 9th Avenue, Fort Lauderdale, FL 33315, USA
[c]Department of Earth Sciences, Florida International University, University Park, Miami FL 33199, USA

Received 1 November 2005; received in revised form 6 April 2006; accepted 6 April 2006

Abstract

SEAWAT is a finite-difference computer code designed to simulate coupled variable-density ground water flow and solute transport. This paper describes a new version of SEAWAT that adds the ability to simultaneously model energy and solute transport. This is necessary for simulating the transport of heat and salinity in coastal aquifers for example. This work extends the equation of state for fluid density to vary as a function of temperature and/or solute concentration. The program has also been modified to represent the effects of variable fluid viscosity as a function of temperature and/or concentration. The viscosity mechanism is verified against an analytical solution, and a test of temperature-dependent viscosity is provided. Finally, the classic Henry–Hilleke problem is solved with the new code.

Keywords: Ground water flow modeling; Solute transport modeling; Heat transport modeling; Seawater intrusion

1. Introduction

The density and viscosity of fluids vary with temperature. In computational hydrogeology such variations historically have been assumed to be minor and were largely ignored. However, there is now an increasing need to simulate the effects of direct manipulation of ground water systems where significant temperature differences might exist (e.g., aquifer storage and recovery, deep well waste injection, ground source heat pumps) and a need for more resolution in critical ground water studies where temperature is likely to play a role (e.g., sole source aquifers, coastal aquifer/ocean interactions). The increasing availability of adequate computational resources also has made such simulations accessible to a much broader set of potential users.

SEAWAT (Guo and Bennett, 1998; Guo and Langevin, 2002; Langevin et al., 2003), couples MODFLOW (Harbaugh et al., 2000) and MT3DMS (Zheng and Wang, 1999) to simulate variable density ground water flow. In previous SEAWAT versions, users could simulate transport of multiple chemical species, but fluid density was calculated as a function of solute concentration for only a single species (e.g., salinity, chloride, or

☆Software available at http://www.iamg.org/. For future updates see http://water.usgs.gov/ogw/seawat/

*Corresponding author. Tel.: +1 305 348 3117; fax: +1 305 348 3877.
E-mail address: sukopm@fiu.edu (M.C. Sukop).

0098-3004/$ - see front matter © 2006 Elsevier Ltd. All rights reserved.
doi:10.1016/j.cageo.2006.04.005

relative seawater fraction). Furthermore, previous versions of SEAWAT did not represent the effects of fluid viscosity variations, which can be important for problems with large temperature or salinity variations.

This paper documents enhancements to the SEAWAT computer code, which allow it to represent the simultaneous transport of solutes and heat. To simulate heat transport within the context of the SEAWAT framework, one of the MT3DMS species is used to represent temperature. The effect of temperature variations on ground water flow is included in the new program by modifying the density equation of state to vary with the temperature T of the fluid as well as the concentration C of a solute. In particular, the new equation of state is

$$\rho(C,T) = \rho_f + \frac{\partial \rho}{\partial C}(C - C_0) + \frac{\partial \rho}{\partial T}(T - T_0), \qquad (1)$$

where the density of freshwater ρ_f, the change in density with respect to concentration and temperature $\partial\rho/\partial C$ and $\partial\rho/\partial T$, and C_0 and T_0 are prescribed constants input by the user. The effect of viscosity variations on the resistance to ground water flow also was added through implementation of the relationship between permeability, viscosity, and hydraulic conductivity. Viscosity is incorporated into the flow equation as a function of both temperature and solute concentration (or just one or the other, as desired). A variety of published formulas for viscosity is supported by the new program (Holzbecher, 1998; Johannsen et al., 2002; Hughes and Sanford, 2004) but they are not described here.

Examples verifying the temperature component and variable viscosity mechanism are shown. The paper culminates with our solution of the Henry–Hilleke problem, a seawater intrusion scenario involving the full equation of state, Eq. (1).

2. Mathematical approach

Two new capabilities are introduced to SEAWAT: (1) simultaneous transport of energy and solute; and (2) representation of fluid viscosity variations. MT3DMS was designed to simulate solute transport; however, the code also has been used to simulate heat transport (e.g. Martin et al., 2001). Here, we briefly introduce the analogy between solute and energy transport. Then we give a brief discussion of the role of variable viscosity in Darcy's law and its implementation.

2.1. Solute transport

Among the forms of the advection–dispersion equation solved by MT3DMS is (Zheng and Wang, 1999):

$$\left(1 + \frac{\rho_b K_d}{\theta}\right)\frac{\partial(\theta C^k)}{\partial t} = \frac{\partial}{\partial x_i}\left(\theta D_{ij}\frac{\partial C^k}{\partial x_j}\right) - \frac{\partial}{\partial x_i}(\theta v_i C^k) + q_s C^k_s + \sum R_n, \qquad (2)$$

where ρ_b is porous medium bulk density, K_d is the linear sorption coefficient (distribution coefficient), θ is the volumetric water content, C^k is the concentration of species k, t is time, x_i is the i^{th} spatial coordinate, D_{ij} is the diffusion–dispersion tensor, v_i is the mean pore water velocity vector, q_s is a source or sink volumetric flow rate per unit volume, $C^k{}_s$ is a source or sink concentration, and R_n is a reaction term considering first order production or decay.

The time derivative on the left hand side of Eq. (2) represents the change in total solute mass per unit volume of aquifer with respect to time. Diffusive and dispersive processes are contained in the first term on the right hand side. The second term on the right hand side is the advection term. The third term accounts for sources and sinks whereas the fourth term incorporates chemical reactions. Eq. (2) is solved by the MT3DMS routines in SEAWAT to simulate the transport of salinity or other solutes that might lead to nonuniform solution densities and a subsequent effect on flow (Langevin et al., 2003). We wish to leverage this equation to solve energy transport, which is analogous to solute transport in several ways (e.g., Voss, 1984; Martin et al., 2001; Kim et al., 2005).

2.2. Energy transport

Key parameters in energy transport processes are thermal conductivity, k_T, and specific heat capacity, c_P. In a way analogous to the hydraulic conductivity in Darcy's law or the diffusion coefficient in Fick's law, the thermal conductivity, k_T, is used in Fourier's law for heat transport:

$$q_T = -k_T \frac{\partial T}{\partial x}. \qquad (3)$$

The thermal conductivity is assumed to be isotropic and has units of energy per unit time, length, and temperature (e.g., $Wm^{-1}{}^{\circ}C^{-1}$). Thus, the heat flux, q_T, has units of Wm^{-2}. Unlike solutes, where movement is essentially confined to fluid phases, energy also is transported through aquifer solids by conduction (controlled by the thermal conductivity of the solids). Hence, we have new parameters, k_{Tfluid} and k_{Tsolid}, to distinguish the thermal conductivities of the fluid and solid phases.

Heat is stored in the fluid and solid phases according to their specific heat capacities, c_{Pfluid} and c_{Psolid}, which relate the temperature to energy stored at constant pressure. Heat capacity has units of energy per unit mass and temperature (e.g., $J\,kg^{-1}\,{}^{\circ}C^{-1}$). For solutes, the prefactor of the time derivative in Eq. (2) can account for both the dissolved and adsorbed solute. In the case of heat, the prefactor similarly accounts for the change in heat storage in both the fluid and solid phases. In the fluid phase, the energy stored is given by the temperature of the fluid multiplied by its volume, heat capacity, and density, which is $\theta c_{Pfluid}\rho T$, whereas the energy stored in the solids is given by the temperature multiplied by the solid volume, heat capacity, and density, which is $(1–\theta)c_{Psolid}\rho_s T$.

For solutes in water, the advective component is simply vC, but for heat we need to relate the temperature to the heat energy stored in the flowing fluid. Because v is the volumetric flux and c_P is on a unit mass basis, we need to multiply by density to convert volumetric flux to mass flux of liquid. Thus the advective heat flux in the moving water is $v\rho c_{Pfluid}T$. The dispersive heat flux involves the same factors and is $\partial\left[\rho c_{Pfluid}D_{ij}(\partial T/\partial x_j)\right]/\partial x_i$.

An equation that incorporates these processes is (Kipp, 1987; Voss and Provost, 2003; Hughes and Sanford, 2004)

$$\begin{aligned}&\frac{\partial}{\partial t}\left(\left[\theta\rho c_{Pfluid}+(1-\theta)\rho_s c_{Psolid}\right]T\right)\\&=\frac{\partial}{\partial x_i}\left(\left\{\left[\theta k_{Tfluid}+(1-\theta)k_{Tsolid}\right]\mathbf{I}+\theta\rho c_{Pfluid}D_{ij}\right\}\frac{\partial T}{\partial x_j}\right)\\&\quad-\frac{\partial}{\partial x_i}\left(\theta\rho c_{Pfluid}v_i T\right)+q_s\rho c_{Pfluid}T_s\\&\quad+\theta\rho\gamma_{fluid}+(1-\theta)\rho_s\gamma_{solid},\end{aligned}\tag{4}$$

where $\mathbf{I}$ is the identity tensor, D_{ij} is now the dispersion tensor, and γ_{fluid} and γ_{solid} are zero-order rate constants for heat production or loss (energy per unit time and mass of fluid and solid respectively; e.g., $W\,kg^{-1}$). We write this equation so there is a one-to-one correspondence between its terms and the terms in Eq. (2), although the reaction term has been split into two parts involving zero order production or loss in the fluid and solid phase, respectively.

Eq. (4) makes it clear that it is energy being transported rather than just temperature. The first term describes the time rate of change of energy stored in both the fluid and solid phases. The second term describes both the conductive and dispersive energy fluxes. The conduction is assumed to be isotropic and hence involves the identity tensor $\mathbf{I}$. It is possible to consider the fluid and solid phase thermal conductivities, k_{Tfluid} and k_{Tsolid}, separately or combine them into a bulk value using one of several available 'mixing' models (e.g., Clauser and Huenges, 1995; Hughes and Sanford, 2004); the simplest of these is to weight the fluid thermal conductivity by the volumetric fluid content and add it to the solid conductivity weighted by the volumetric solids fraction. For a saturated porous medium, we then have $k_{Tbulk}=\theta k_{Tfluid}+(1–\theta)k_{Tsolid}$.

Like existing models that address energy transport (e.g., SUTRA, HST3D), dispersive energy transport is assumed here; as in solute transport, it accounts for the fact that the mean ground water velocity used in Darcy's law is only an average of the detailed pore velocities. Thus, the treatment is that of anisotropic mechanical heat dispersion governed by a saturated aquifer thermal diffusivity tensor (D_{ij} in Eq. (4)). Heat conduction is governed by the bulk thermal diffusivity, which is analogous to the solute diffusion coefficient. In the present formulation, the bulk thermal diffusivity is a combination of both the water and solid phases.

Finally, we utilize the Oberbeck-Boussinesq approximation (e.g., de Marsily, 1986; Holzbecher, 1998; Kolditz et al., 1998; Nield and Bejan, 1999) to assume constant fluid density, ρ, within the transport equation, which leads to considerable simplification. This assumption in the context of a density-dependent model is not as radical as it might seem. In each instance that this assumption is applied to the energy transport equation, it is in the context of the energy content and appears as $c_{Pfluid}\rho T$. If the maximum likely difference in density is comparable to that between fresh and seawater (2.5%), then the error in energy transport should be similarly small. With this assumption, ρ (and c_{Pfluid}) can be factored out of the derivatives and we can

rewrite Eq. (4) as:

$$\left(1+\frac{1-\theta}{\theta}\frac{\rho_s}{\rho}\frac{c_{Psolid}}{c_{Pfluid}}\right)\frac{\partial(\theta T)}{\partial t} = \frac{\partial}{\partial x_i}\left(\theta\left[D^* + D_{ij}\right]\frac{\partial T}{\partial x_j}\right) - \frac{\partial}{\partial x_i}(\theta v_i T) + q_s T_s + \frac{\theta\gamma_{fluid}}{c_{Pfluid}} + \frac{(1-\theta)\gamma_{solid}}{c_{Pfluid}}\frac{\rho_s}{\rho}, \quad (5)$$

which is basically Eq. (2) with substitution of T for C^k. The coefficient on the time derivative represents heat stored in both the fluid and solid phases and corresponds to the retardation factor for sorbed solutes where the key equivalence that must be established is

$$K_d = \frac{1}{\rho}\frac{c_{Psolid}}{c_{Pfluid}}.$$

This equation was determined by equating the prefactors of the time derivatives in Eqs. (2) and (5) and solving for K_d. We can estimate the retardation of heat energy transport under different circumstances by considering the c_p values for water, quartz, and calcite, which are 4183, 652, and 8350 $J\,kg^{-1}\,K^{-1}$, respectively, and the density values, which are 1000, 2643, and 2710 $kg\,m^{-3}$, respectively. If we assume $\theta = 0.35$ as a representative, constant value, then the "Kds" that would be put into the model are about 1.6×10^{-4} and 2.0×10^{-4} $m^3\,kg^{-1}$ and the resulting heat energy retardation factors are about 1.8 and 2.0 for quartz and calcite aquifers respectively.

The standard solute transport model diffusion coefficient, D^*, is replaced with the bulk thermal diffusivity, $D^* = k_{Tbulk}/\theta\rho c_{Pfluid}$. We can compute the approximate thermal diffusivity, D^*, for quartz and calcite aquifers using the k_T values for water, quartz, and calcite (0.61, 7.69, and 3.59 $W\,m^{-1}\,K^{-1}$, respectively) and assuming as above that $\theta = 0.35$ and $\rho = 1000\,kg\ m^{-3}$. We obtain $3.7\times10^{-6}\,m^2s^{-1}$ for quartz aquifers and $1.7\times10^{-6}\,m^2s^{-1}$ for calcite aquifers. These values are 3 orders of magnitude larger than diffusion coefficients for solutes in water.

Because the zero order heat production and decay are essentially distributed source/sinks, they can be combined with the preexisting source/sink term q_sT_s by simply adding a

$$q_s'T_s' = \frac{\theta\gamma_{fluid}}{c_{Pfluid}} + \frac{(1-\theta)\gamma_{solid}}{c_{Pfluid}}\frac{\rho_s}{\rho}\ \text{term}.$$

Eq. (5) and the equivalences noted here encapsulate the current SEAWAT implementation of energy transport based on an MT3DMS species.

For most purposes, the approximations employed in the development of the extended SEAWAT are not expected to lead to significant error, but for certain conditions they may not accurately reflect the physical processes that may be occurring. Voss and Provost (2002) provide additional discussion on the use of the dispersion approach for heat.

2.3. Variable viscosity

Darcy's law, as written in the MODFLOW user's guide (Harbaugh et al., 2000), is $Q = COND(h_A - h_B)$ where, for the extended SEAWAT, the conductance $COND$ is expanded as

$$COND = \frac{\mu_f}{\mu}\frac{T^*W}{L}. \quad (6)$$

or in terms of hydraulic conductivity instead of transmissivity

$$COND = \frac{\mu_f}{\mu}\frac{KWB}{L}, \quad (7)$$

where h is hydraulic head, T^* is transmissivity, W is width of the cell, L is length of the cell, K is hydraulic conductivity, and B is height of the cell. SEAWAT is formulated using "equivalent freshwater" hydraulic conductivity and transmissivity values (Guo and Langevin, 2002). Thus, the T^* and K values used in Eqs. (6) and (7) represent an aquifer that is saturated with the reference fluid at the reference temperature (normally assumed to be freshwater at 25 °C).

The ratio μ_f/μ accounts for variation in viscosity $\mu = \mu(C,T)$ from some reference viscosity μ_f. When $\mu > \mu_f$, conductance $COND$ is lower than in the isoviscous case, and when $\mu < \mu_f$ the conductance $COND$ is higher than in the isoviscous case.

2.3.1. Horizontal conductance

Horizontal conductance is conductance between adjacent cells across rows or columns. In the present version of SEAWAT, horizontal conductance is calculated using one of two methods for calculating the interblock transmissivity. The most common method is based on harmonic mean averaging, which assumes a piece-wise constant transmissivity distribution. The logarithmic mean also can be used for interblock averaging if it can be assumed that transmissivity varies linearly between cells. As an

example, suppose cells 1 and 2 are adjacent across either rows or columns. To compute the conductance, *COND*, between two cells, Eq. (6) is first used to calculate the conductance for the two adjacent half-cells:

$$C_1 = \frac{\mu_f}{\mu_1}\frac{T_1^* W}{\frac{1}{2}L_1} \quad \text{and} \quad C_2 = \frac{\mu_f}{\mu_2}\frac{T_2^* W}{\frac{1}{2}L_2}. \tag{8}$$

If the harmonic mean method is selected, for example, then these conductances are substituted into $COND = C_1C_2/(C_1 + C_2)$ (Eq. 13 in the MODFLOW user's guide (Harbaugh et al., 2000)) to obtain, with some simplification,

$$COND = 2\mu_f W \frac{T_1^* T_2^*}{T_1^*\mu_2 L_2 + T_2^*\mu_1 L_1}. \tag{9}$$

2.3.2. Vertical conductance

Vertical conductance is calculated using the harmonic average between cells that are adjacent across layers. Suppose cells 1 and 2 are adjacent across layers. To compute the conductance, *COND*, between the cells, substitute the conductances, Eq. (7), of the two adjacent half-cells:

$$C_1 = \frac{\mu_f}{\mu_1}\frac{K_1 WL}{\frac{1}{2}B_1} \quad \text{and} \quad C_2 = \frac{\mu_f}{\mu_2}\frac{K_2 WL}{\frac{1}{2}B_2}, \tag{10}$$

into $COND = C_1C_2/(C_1 + C_2)$ This gives, after some simplification,

$$COND = 2\mu_f WL \frac{K_1K_2}{K_1\mu_2 B_2 + K_2\mu_1 B_1}. \tag{11}$$

3. Examples

We present three examples here. The first example is contrived to verify the variable viscosity feature on its own, and is compared with an analytical solution. The second example explores temperature dependent viscosity, and is compared with results from a previous version of SEAWAT solving an equivalent problem with variable conductivity instead of viscosity. The last example is the Henry–Hilleke problem (Henry and Hilleke, 1972), and is compared with previously published results.

The thermal component and the variable viscosity mechanism are implemented in a general fashion allowing temperature to be interpreted as a second solute component, further broadening the potential uses of the extended SEAWAT. The following examples introduce and verify the new software, but many other types of simulations are possible. In particular Diersch and Kolditz (1998) present FEFLOW results of simulations for thermohaline versions of the Elder and salt dome problems as well as a three-dimensional extension of the Elder problem including thermal effects. These problems could potentially serve as additional benchmark problems for the extended SEAWAT model.

3.1. Prescribed viscosity gradient

This example considers the effect of a prescribed viscosity gradient on the resulting head gradient. We expect the effect of a viscosity gradient to be the same as the effect of a corresponding equivalent freshwater hydraulic conductivity gradient (effectively an intrinsic permeability gradient) in the opposite direction. In addition to being a concise way of verifying the new viscosity mechanism by comparing it with the existing conductivity mechanism, this problem is compelling because it has an analytical solution that can be derived as follows. This is a problem of one-dimensional Darcy flow between two fixed heads with a simple linear hydraulic conductivity gradient chosen as $K(x) = x$, which applies for all $x > 0$. Darcy's law is then $q = -x(dh/dx)$. Incorporating this into the continuity equation

$$\mathrm{d}q/\mathrm{d}x = 0 \text{ yields } \frac{\mathrm{d}\left(-x(\mathrm{d}h/dx)\right)}{\mathrm{d}x} = 0.$$

One integration gives $-x\ \mathrm{d}h/\mathrm{d}x + A = 0$ and then separation of variables gives $\mathrm{d}h = A/x\,\mathrm{d}x$, which can be integrated again to give a solution for head $h = A\ln x + B$. Finally, incorporating the boundary conditions $h(\mathrm{x}_{\min}) = h_0$ and $h(\mathrm{x}_{\max}) = h_1$ leads to

$$h = \frac{h_1 - h_0}{\ln(x_{\max}) - \ln(x_{\min})}[\ln(x) - \ln(x_{\min})] + h_0, \tag{12}$$

where h_0 and h_1 are the prescribed heads at the end points.

We run two cases: (a) a variable viscosity with constant permeability that gives a linear conductance gradient; and (b) a variable permeability with constant viscosity that gives the same linear conductance gradient. For both cases, the logarithmic mean interblock transmissivity method was used for calculating horizontal conductance. This allows the numerical results to be compared directly with the analytical solution, which is based on a linear hydraulic conductivity variation. The resulting heads (Fig. 1) are identical in both cases as expected and follow the analytical solution closely.

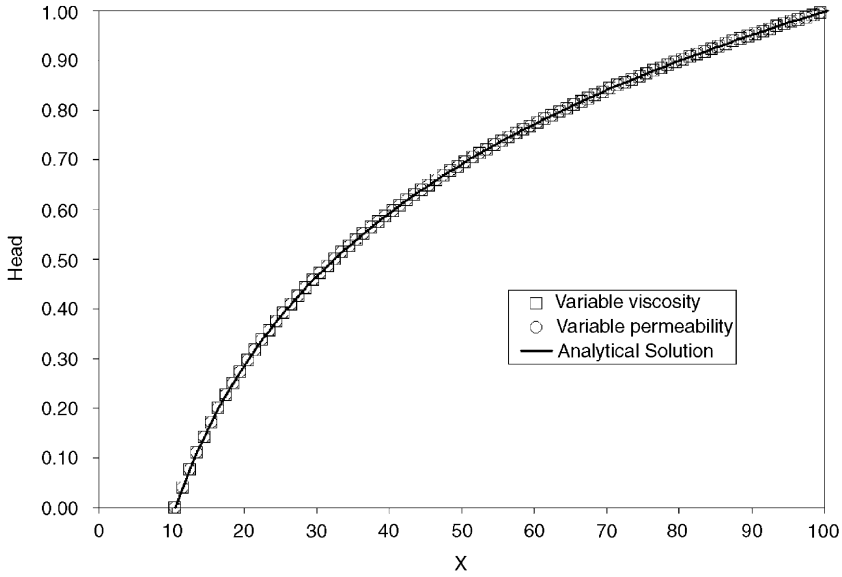

Fig. 1. Verification of viscosity mechanism. Hydraulic conductivity is varied linearly across domain by varying either intrinsic permeability or viscosity. Simulations and analytical solution for constant head boundaries, $h_{10.5} = 0$ and $h_{100.5} = 1$, are shown.

This represents complete verification of the viscosity mechanism. The test shows that the viscosity is being stored and used correctly and that it is properly incorporated into the conductance term. This test has a shortcoming though; viscosity is prescribed, so its dependence on temperature and/or salinity is not tested. This is addressed in the next example.

3.2. Temperature-dependent viscosity gradient

Viscosity and intrinsic permeability or equivalent freshwater hydraulic conductivity have inversely proportional effects on conductance. The effect of a given viscosity gradient on head corresponds to the effect of a predictable permeability gradient. The previous example shows that SEAWAT simulates this effect properly; however, it did not test the way that viscosity is dependent on temperature and/or concentration. This test, on the other hand, incorporates temperature-dependent viscosity. We begin by running a case with constant temperature boundaries at the ends of the domain. This results in a temperature gradient that induces variable viscosity across the domain. We then compute a variable conductivity that mirrors the variable viscosity of the first case and run an isothermal case (hence, constant viscosity) with variable permeability that mimics the effect of viscosity in the first case. The viscosity function is $\mu(x) = \mu_f - (\mathrm{d}\mu/\mathrm{d}T)T(x)$. For convenience, this is a simple linear relationship with temperature, where $\mu_f = 13$ and $\mathrm{d}\mu/\mathrm{d}T = 0.1$. For the variable conductivity simulation, $K(x) = K_0\mu_f/\mu(x)$, where K_0 is an arbitrary reference conductivity. The head distributions computed by the different methods are the same, as shown in Fig. 2. These results confirm that the temperature-dependent viscosity implementation functions as expected.

3.3. Henry–Hilleke problem

The Henry problem (Henry, 1964) is a classic variable density flow problem, which is of particular interest in the context of saltwater intrusion along coastal areas. SEAWAT results for the Henry problem have been previously published (Guo and Langevin, 2002). In 1972, Henry and Hilleke evaluated the effects of temperature-dependent density on coastal ground water flow (Henry and Hilleke, 1972). Since that time, HST3D and the recently developed SUTRA-MS have been tested using this problem (Hughes and Sanford, 2004), and we compare our results to the SUTRA-MS solution here.

The Henry–Hilleke problem domain is rectangular and the problem has been simulated at a variety of aspect ratios. We present results for a square 1m-by-1m domain. In keeping with previous literature (Henry and Hilleke, 1972; Hughes and Sanford,

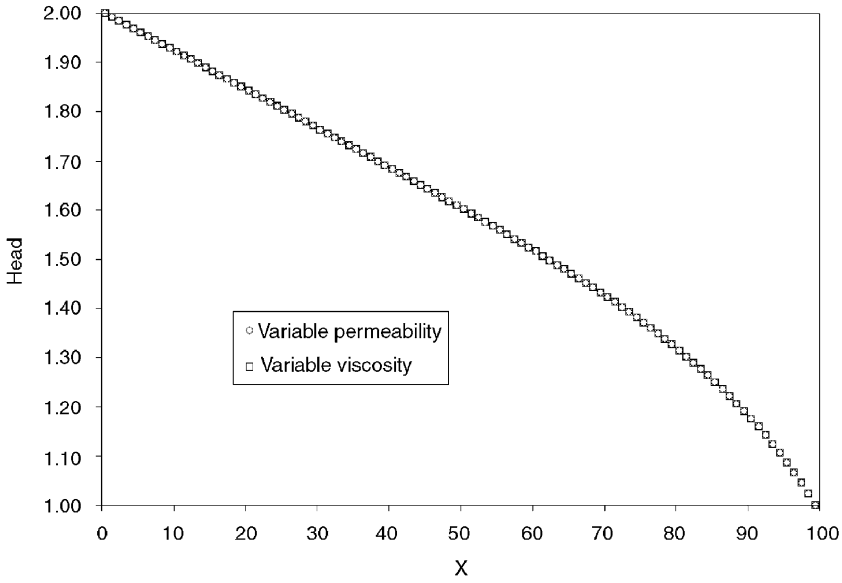

Fig. 2. Temperature-dependent viscosity. Temperature gradient across domain causes a viscosity gradient that leads to a nonlinear head gradient. A comparable simulation mimics expected effect of varying viscosity by varying permeability alone.

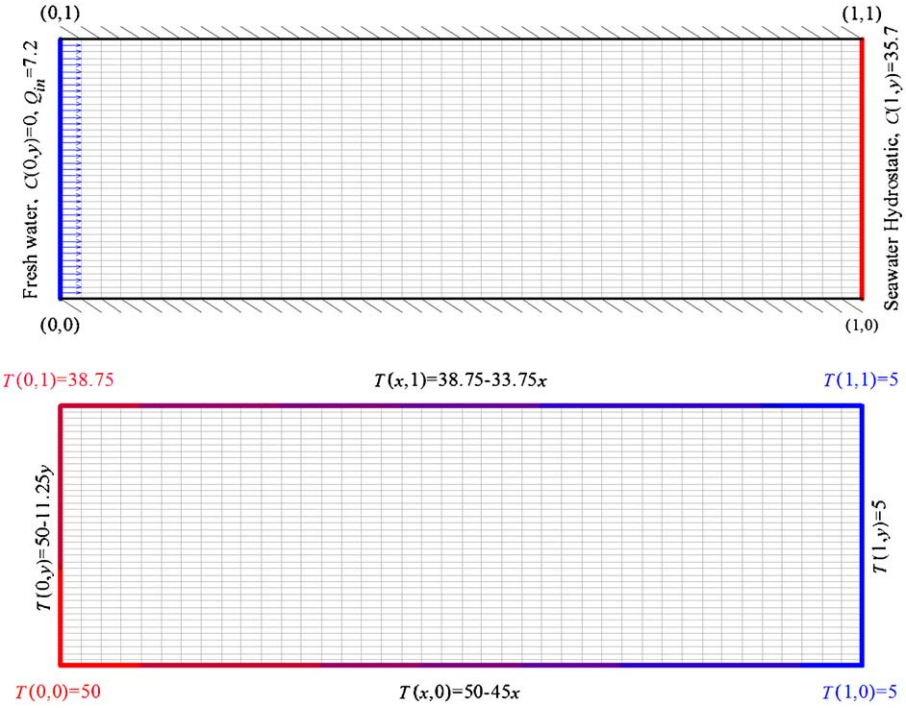

Fig. 3. Domain with flow and concentration boundary conditions (top) and temperature boundary conditions (bottom). Flow in $m^3 d^{-1}$. Temperature in °C.

2004), concentration and temperature contour plots are shown on a grid reduced by a factor of 3 in the vertical direction. We show our results overlying the SUTRA-MS results. HST3D results are very similar to the SUTRA-MS results as shown by Hughes and Sanford (2004).

Constant temperature boundary conditions surround the domain. The lower left corner is hot at 50 °C, while the right boundary is cool at 5 °C. There is a linear gradient in temperature from the hot lower left corner to the cool right boundary as shown in Fig. 3. This corresponds

Table 1
Henry–Hilleke parameters

Parameter	Variable	Value
Equivalent freshwater hydraulic conductivity	K	$864\,\mathrm{m\,d^{-1}}$ ($=.01\,\mathrm{m\,s^{-1}}$)
Porosity	θ	0.35
Equivalent freshwater viscosity	μ	$86.4\,\mathrm{kg\ m^{-1}\,d^{-1}}$ ($=.001\,\mathrm{kg\,m^{-1}\,s^{-1}}$)
Molecular diffusion	D_m	$2.0571\,\mathrm{m^2\,d^{-1}}$ ($=2.381\times10^{-5}\,\mathrm{m^2\,s^{-1}}$)
Thermal diffusivity	D^*	$20.571\,\mathrm{m^2\,d^{-1}}$ ($=2.381\times10^{-4}\,\mathrm{m^2\,s^{-1}}$)
Longitudinal dispersivity	α_l	0 m
Transverse dispersivity	α_t	0 m
Inflow	Q_{in}	$7.2\,\mathrm{m^3\,d^{-1}}$ $=$ (41 nodes)$(0.1756\,\mathrm{m^3\ d^{-1}})$ ($=8.333\times10^{-5}\,\mathrm{m^3\,s^{-1}}$)
Salinity concentration in freshwater	C_f	$0\,\mathrm{kg\,m^{-3}}$
Salinity concentration in sea water	C_s	$35.7\,\mathrm{kg\,m^{-3}}$
Density of freshwater	ρ_f	$1000\,\mathrm{kg\,m^{-3}}$
Density of sea water	ρ_s	$1025\,\mathrm{kg\,m^{-3}}$
Density change with concentration	$\mathrm{d}\rho/\rho C$	0.7
Density change with temperature	$\mathrm{d}\rho/\mathrm{d}T$	$-0.375\,\mathrm{kg\,m^{-3}\,°C^{-1}}$

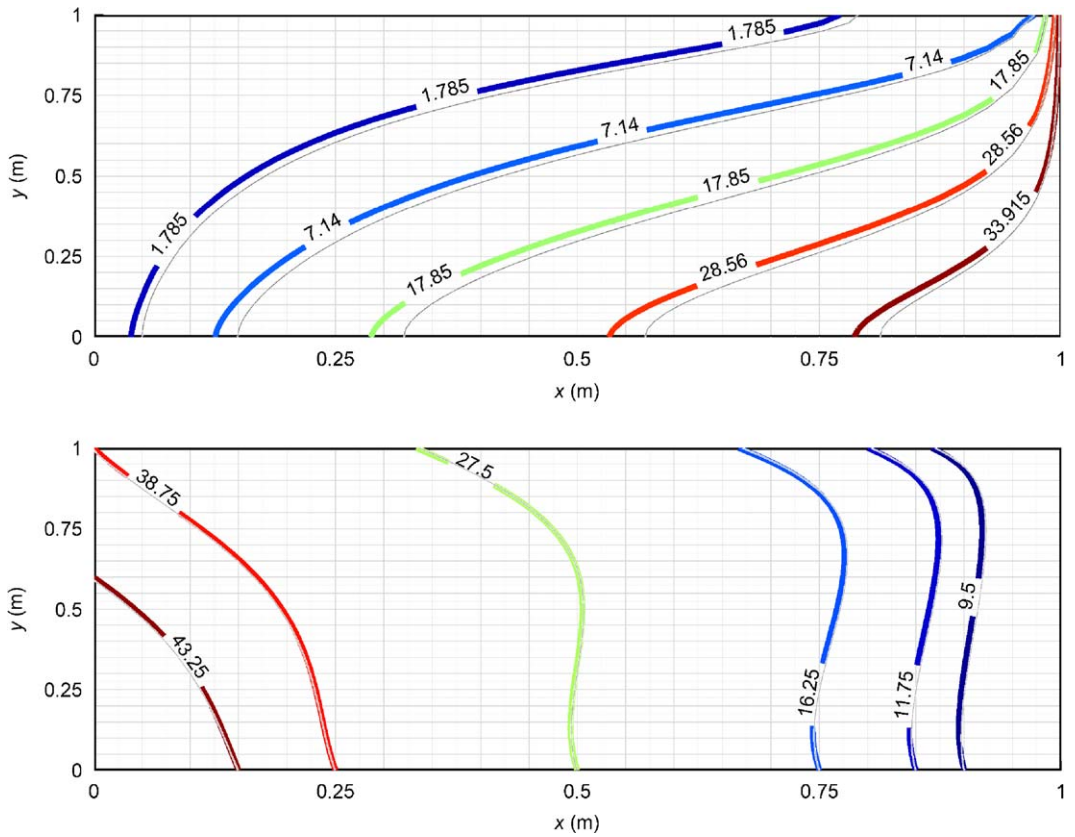

Fig. 4. Isochlors (top) and isotherms (bottom). New SEAWAT results in thick colored contours. SUTRA-MS in thin gray contours. Initial simulation results. (Isochlors plotted at $C = 35.7*[.05\ .2\ .5\ .8\ .95] = [1.7850\ 7.1400\ 17.850\ 28.560\ 33.915]\,\mathrm{kg\,m^{-3}}$. Isotherms plotted at $T = [43.25\ 38.75\ 27.5\ 16.25\ 11.75\ 9.5]$°C.)

to warm subterranean freshwater and cool seawater.

For the Henry–Hilleke problem, the equation of state is:

$$\rho(C,T) = \rho_f + \frac{d\rho}{dC}C + \frac{d\rho}{dT}T, \quad (13)$$

where $\rho_f = 1000\,\mathrm{kg\,m^{-3}}$, $d\rho/dC = 0.7$, and $d\rho/dT = -0.375\,\mathrm{kg\,m^{-3}\,^{\circ}C^{-1}}$. The effects of variable viscosity are not represented.

The grid is 41-by-41 cells with $dx = dy = 0.025\,\mathrm{m}$. This actually gives a slightly larger than 1m-by-1m domain, but allows our cell-centered finite difference grid points to exactly overlay the SUTRA finite element node points. We run the simulation for about 0.5 days with time steps of 0.00069444 days (= 60 s), which is long enough for equilibration in all cases shown here. The full set of parameters is shown in Table 1.

Fig. 4 shows the initial simulation results. Contours of constant salinity concentration (referred to as isochlors here) are plotted on top and isotherms are plotted on the bottom. The new SEAWAT results are plotted as thick colored contours. The SUTRA-MS results are plotted as thin gray contours. The isochlors are plotted for concentrations $C = 35.7[0.05, 0.2, 0.5, 0.8, 0.95] = [1.7850, 7.1400, 17.850, 28.560, 33.915]\,\mathrm{kg\,m^{-3}}$. The isotherms are plotted for temperatures $T = [43.25, 38.75, 27.5, 16.25, 11.75, 9.5]\,^{\circ}\mathrm{C}$.

The isochlors deviate slightly from what we expect based on SUTRA-MS results. This may be because our boundary conditions are enforced inside of cells that participate in the flow, whereas the SUTRA boundary conditions are enforced on the literal edge of the domain. To test this conjecture, we present a second set of results with a minor modification to the upper and lower layers of boundary cells. In this run, the hydraulic conductivities in those boundary cells are reduced by a factor of two to minimize the advective flux. The result of that modification is shown in Fig. 5.

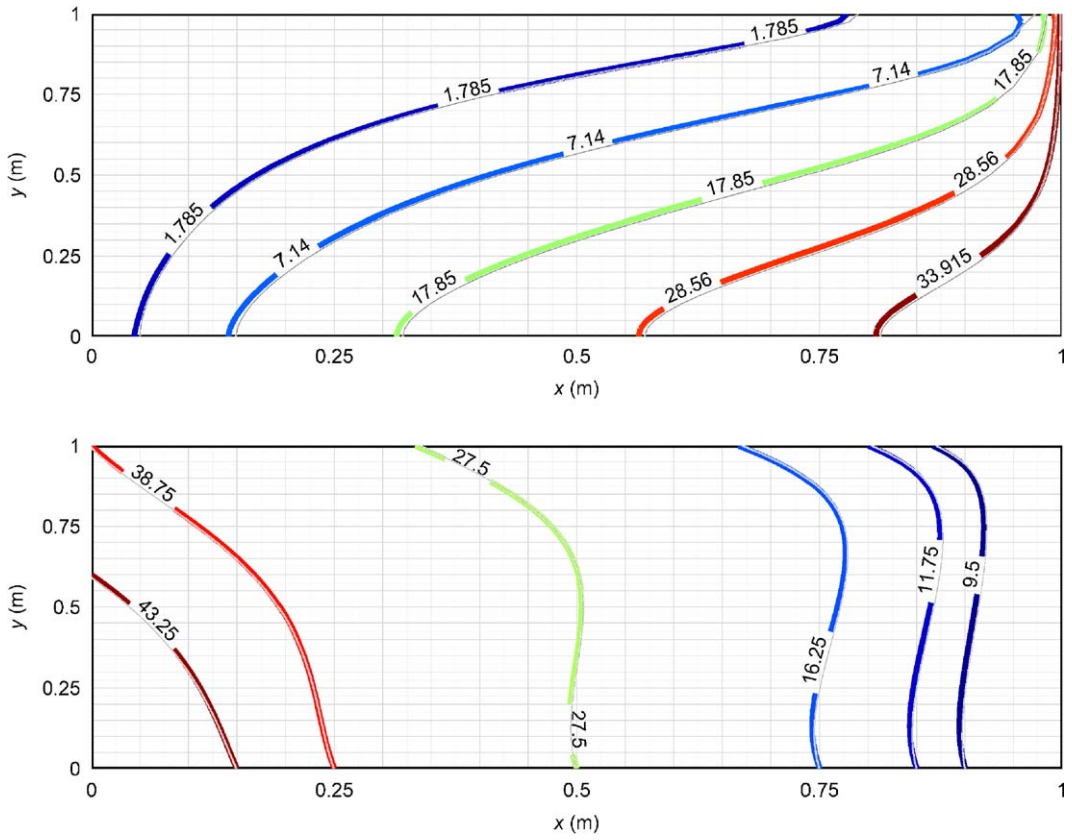

Fig. 5. Isochlors (top) and isotherms (bottom). New SEAWAT results in thick colored contours. Simulation modified with low conductivity along upper and lower sides of the domain. (Isochlors plotted at $C = 35.7*[.05\ .2\ .5\ .8\ .95] = [1.7850\ 7.1400\ 17.850\ 28.560\ 33.915]\,\mathrm{kg\,m^{-3}}$. Isotherms plotted at $T = [43.25\ 38.75\ 27.5\ 16.25\ 11.75\ 9.5]^{\circ}\mathrm{C}$.)

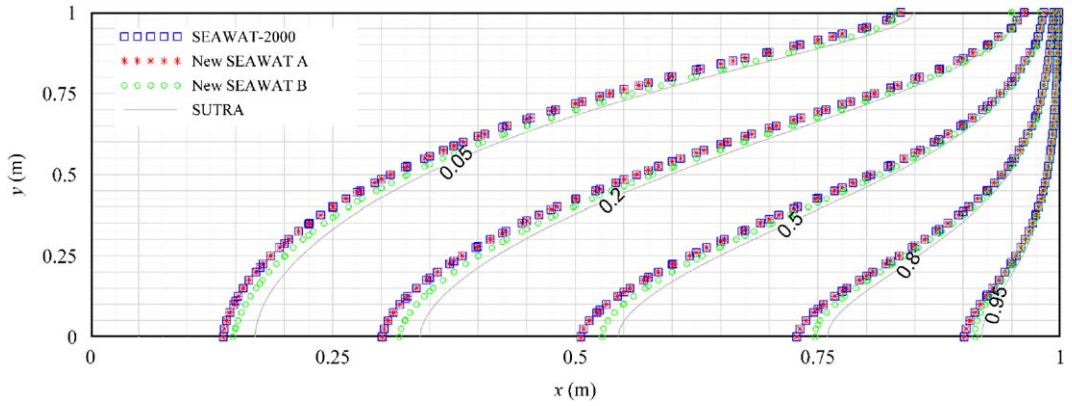

Fig. 6. Isochlors for isothermal case. This shows first that new SEAWAT (New SEAWAT A) gives same result as original SEAWAT (SEAWAT-2000). Second, it shows that applying lower conductivity to upper and lower boundary rows (New SEAWAT B) brings our contours closer to SUTRA-MS contours. Thirdly, it provides a reference case for comparison to full thermal case above.

Indeed, this gives a much better match with the SUTRA-MS results. There is a difference in the isochlors near the upper right corner, but it is relatively minor. Further reducing the conductivities along the upper and lower boundaries does not substantially improve the overall results, but exacerbates the artifact at the upper right corner. Further adjustments to the grid and boundary conditions might eliminate this artifact while preserving the excellent fit.

Another possibility is that differences between the SUTRA-MS and SEAWAT solutions stem from differences in concentration units. SUTRA-MS uses mass fraction concentrations, whereas MT3D-MS and hence SEAWAT use mass/volume concentrations.

Fig. 6 shows isochlors for the isothermal case for comparison with the above thermal case. In addition to serving as a reference case, this also confirms an important point about the new SEAWAT code. Namely, it shows that the new SEAWAT with $\partial\rho/\partial T = 0$ (called SEAWAT A) gives the same result as a previously released version of SEAWAT (SEAWAT-2000). The new SEAWAT run is from the exact same configuration of the SEAWAT/MODFLOW/MT3D input files as the above thermal runs except for the parameter $d\rho/dT$. Another item of interest that is illustrated by this plot is that enforcing the low conductivity rows along the upper and lower boundary brings our contours (SEAWAT B) closer to the SUTRA contours as in the full thermal case above.

4. Conclusions

The new version of SEAWAT introduced here is capable of simulating the simultaneous transport of heat and solute. The effect of temperature on fluid density is included through the addition of a new term to the equation of state. The new model also simulates the temperature and salinity dependence of viscosity. A number of initial test cases verify the new capabilities of the code. Comparison with the results of SUTRA-MS, which is capable of similar simulations, is good suggesting consistency with previous efforts. A key advantage of SEAWAT is that it is based on the widely used MODFLOW/MT3D packages and users of those models should find it straightforward to use.

Appendix A. Supplementary materials

Supplementary data associated with this article can be found in the online version at doi:10.1016/j.cageo.2006.04.005

References

Clauser, C., Huenges, E., 1995. Thermal conductivity of rocks and minerals. In: Ahrens, T.J. (Ed.), Rock Physics and Phase Relations: A Handbook of Physical Constants. American Geophysical Union, Washington, DC, pp. 105–126.

de Marsily, G., 1986. Quantitative Hydrogeology: Groundwater Hydrology for Engineers. Academic Press, London, 464 pp.

Diersch, H.-J.G., Kolditz, O., 1998. Coupled groundwater flow and transport: 2. Thermohaline and 3D convection systems. Advances in Water Resources 21, 401–425.

Guo, W., Bennett, G.D., 1998. SEAWAT version 1.1: A computer program for simulations of groundwater flow of variable density. Missimer International, Inc., Fort Myers, FL.

Guo, W., Langevin, C.D., 2002. User's guide to SEAWAT: A computer program for simulation of three-dimensional variable-density ground-water flow US Geological Survey Techniques of Water Resources Investigations 6-A7, Tallahassee, FL 77 pp.

Harbaugh, A.W., Banta, E.R., Hill, M.C., McDonald, M.G., 2000. MODFLOW-2000, The US Geological Survey modular ground-water model—User Guide to modularization concepts and the ground-water flow process. US Geological Survey, Reston, VA, 121 pp.

Henry, H.R., 1964. Effects of dispersion on salt encroachment in coastal aquifers: US Geological Survey Water-Supply Paper, 1613-C. US Geological Survey, Reston, VA, pp.C71–C84.

Henry, H.R., Hilleke, J.B., 1972. Exploration of multiphase fluid flow in a saline aquifer system affected by geothermal heating, University of Alabama Bureau of Engineering Research Contract No. 14-08-0001-12681. US Geological Survey, Washington DC, 105 pp, submitted for publication.

Holzbecher, E., 1998. Modeling Density-Driven Flow in Porous Media: Principles, Numerics, Software, Springer, Berlin, Heidelberg, 286 pp.

Hughes, J.D., Sanford, W.E., 2004. SUTRA-MS, A version of SUTRA modified to simulate heat and multiple-solute transport. US Geological Survey Open File Report 2004-1207. US Geological Survey, Reston, VA, 141 pp.

Johannsen, K., Kinzelbach, W., Oswald, S., Wittum, G., 2002. The saltpool benchmark problem—Numerical simulation of saltwater upcoming in a porous medium. Advances in Water Resources 25, 335–348.

Kim, J., Park, Y., Harmon, T.C., 2005. Real-time model parameter estimation for analyzing transport in porous media. Ground Water Monitoring & Remediation 25, 78–86.

Kipp, Jr., K.L., 1987. HST3D: A computer code for the simulation of heat and solute transport in three-dimensional ground-water flow systems. US Geological Survey Water-Resources Investigations Report 86-4905. US Geological Survey, Reston, VA, 517 pp.

Kolditz, O., Ratke, R., Diersch, H.J.G., Zielke, W., 1998. Coupled groundwater flow and transport: 1. Verification of variable density flow and transport models. Advances in Water Resources 21, 27–46.

Langevin, C.D., Shoemaker, W.B., Guo, W., 2003. MODFLOW-2000, the US Geological Survey modular ground-water model–documentation of the SEAWAT-2000 version with the variable density flow process (VDF) and the Integrated MT3DMS Transport Process (IMT). US Geological Survey Open File Report 03-426, Tallahassee FL, 43 pp.

Martin, R.J., Bender, S.F., Gaulke, S.W., Wallace, J., 2001. Simulation of groundwater flow and heat transport on Grand Cayman Island. In: Seo, S., Poeter, E.P., Zheng, C., Poeter, O., (Eds.), MODFLOW 2001 and Other Modeling Odysseys, Conference Proceedings. International Ground Water Modeling Center, Colorado School of Mines, Golden, CO, pp.776–782.

Nield, D.A., Bejan, A., 1999. Convection in Porous Media, second ed. Springer, New York, NY, 408 pp.

Voss, C.I., 1984. A finite-element simulation model for saturated-unsaturated, fluid-density-dependent ground-water flow with energy transport or chemically reactive single-species solute transport. USGS Water-Resources Investigations Report 84-4369. US Geological Survey, Reston, VA, 409 pp.

Voss, C.I., Provost, A.M., SUTRA, 2003. A model for saturated-unsaturated, variable-density ground-water flow with solute or energy transport. US Geological Survey Water-Resources Investigations Report 02-4231. US Geological Survey, Reston, VA, 250 pp.

Zheng, C., Wang, P.P., 1999. MT3DMS: A modular three-dimensional multispecies transport model for simulation of advection, dispersion, and chemical reactions of contaminants in groundwater systems; documentation and user's guide, Contract Report SERDP-99-1. US Army Engineer Research and Development Center, Vicksburg, MS, 169 p.